EM2INV – A finite difference based algorithm for two-dimensional inversion of geoelectromagnetic data

P K GUPTA*, SRI NIWAS* and ANUPMA RASTOGI**

*Department of Earth Sciences, University of Roorkee, Roorkee 247667, India.
**Space Application Centre, Ahmedabad, India

The paper presents an efficient finite difference based 2D-inversion algorithm, EM2INV, for geoelectromagnetic data. The special features of the algorithm are

- optimal grid generation based on grid design thumb rules,
- finite domain boundary conditions,
- interpolation matrix that permits generation of response at observation points different from grid points,
- Gaussian elimination forward matrix solver, that enables reuse of already decomposed coefficient matrix,
- super-block notion that reduces the number of blocks with unknown resistivities and, in turn, the size of Jacobian matrix and
- bi-conjugate gradient matrix solver for inverse problem which circumvents the need of explicit Jacobian matrix computation.

The algorithm is tested rigorously by setting up exercises of diverse nature and of practical significance. The stability of the algorithm is established by inverting the synthetic response corrupted with Gaussian noise. The inversion experiments are aimed at studying

- relative performance of response functions,
- inversion quality of E- and B-polarization data,
- efficacy of single and multi-frequency data inversion,
- minimum number of frequencies and observation points needed for successful data inversion.

It has been observed that the Magneto-telluric data deciphers better the vertical position of the target and Geomagnetic Depth Sounding data deciphers the horizontal variations in a better way. The conductive and resistive bodies are better resolved by inversion of E- and B-polarization data respectively. The results of multi-frequency inversion imply that the increase in the number of frequencies does not necessarily enhance the inversion quality especially when the spread of observation points is sufficiently large to sense the target. The study of a minimum number of observation points highlights the importance of single point inversion that furnishes useful information about the inhomogeneity.

1. Introduction

Electromagnetic methods are useful in estimating the spatial variation of subsurface electrical resistivity. A wide range of these methods have been successfully employed in the fields of aeronomy, archaeology, oceanography, environmental and engineering studies, solid earth geophysics and exploration geophysics. The EMSLAB (Electro-Magnetic Sounding of Lithosphere And Beyond) experiment, the largest EM study to date, has played a significant role in popularizing the applicability of these methods

Keywords. 2D inversion; geoelectromagnetic data.

Proc. Indian Acad. Sci. (Earth Planet. Sci.), **108**, No. 4, December 1999, pp. 233–253

(EMSLAB, 1988, 1989). Natural source electromagnetic methods, Magneto-Telluric (MT) and Geomagnetic Depth Sounding (GDS), are deep probing methods that facilitate studies of the earth's internal constitution.

Parameterization of the earth in terms of electrical resistivity has special significance due to its dependence both on chemical composition as well as its thermal state. Resistivity is a good indicator of the distinctive character of materials present, and a knowledge of its spatial distribution provides a clue to the way different kinds of materials are distributed in the deeper regions. The simplest parameterization is the one-dimensional (1D) model wherein resistivity is assumed to vary only with depth. More realistic models of the earth are, however, two-dimensional (2D), where resistivity also varies in one horizontal direction. 2D forward modeling can be performed analytically only for a few idealized models. In general, 2D/3D modeling is performed numerically using the Integral Equation Method (IEM), Differential Equation Method (DEM) and Hybrid Method (HM). Of these, the IEM is the most widely used (Hohmann 1971; Raiche 1974; Reddy *et al* 1977; Ting and Hohmann 1981; Wannamaker *et al* 1984, 1991; Xiong 1992; Zhdanov and Fang 1996). In this method the discretised anomalous region results in a small but full coefficient matrix, and its use is limited to confined targets buried in a layered earth. The DEMs (FDM – Finite Difference Method and FEM – Finite Element Method) are popular for modelling complex geometries. They generate large but grossly sparse coefficient matrices. Advances in iterative solution techniques have made these methods more popular (Sarkar 1991). Easy implementation of FDM makes it more suitable for geophysical problems (Jones and Pascoe 1971; Brewitt-Taylor and Weaver 1976; Mackie *et al* 1993; Smith 1996b; Weaver *et al* 1996). The HM, an amalgamation of IEM and DEM, is suitable only for confined targets (Lee *et al* 1981; Gupta *et al* 1987). Weaver (1994) has described the chronological development of 2D modelling through FDM. Significant progress has also been made in 3D forward modelling, using FDM (Madden and Mackie 1989; Xinghua *et al* 1991; Mackie *et al* 1993; Weaver 1994; Smith 1996a, 1996b).

Solution of the forward problem covers only a part of the quantitative interpretation of EM data. The solution of the inverse problem completes the process. However, the inverse EM problem, being non-linear, is much more difficult to solve in comparison to the linear forward problem. The solution of the non-linear inverse problem can be handled in three different ways:

- transformation of the non-linear problem to a linear one and using a linear inversion technique,
- quasi-linearization of the non-linear problem and using a linear inversion technique in an iterative manner and
- using a non-linear inversion technique.

Several efficient 1D inversion algorithms (Patrick and Bostick 1969; Weidelt 1972; Parker 1977; Oldenburg 1979; Parker and Whaler 1981; Whittall and Oldenburg 1992; Weaver and Agrawal 1993; Gupta *et al* 1996) are available for providing specific 1D models that are consistent with data. However, the existing 2D inversion algorithms (Weidelt 1975; Jupp and Vozoff 1977; Rodi *et al* 1984; Pek 1985; Sasaki 1989; de Groot-Hedlin and Constable 1990; Oldenburg 1990; Smith and Booker 1991; Oldenburg and Ellis 1993; Yamne *et al* 1996) are yet to be rigorously tested on real earth data, whilst 3D inversion algorithms are yet to be fully developed and perfected. This scarcity motivated us to develop a versatile and economically viable inversion algorithm of our own that can provide meaningful information about resistivity variations in the earth from surface measurements. Due to obvious reasons we have restricted our work to 2D inversion only. However, after gaining confidence with this, its extension to 3D problem would not be difficult. The present work has resulted in the development of an efficient finite difference based 2D inversion algorithm christened as EM2INV.

2. The Algorithm – EM2INV

The basis of this finite difference algorithm is the formulation of the forward EM problem given by Brewitt-Taylor and Weaver (1976). Here the domain of study is discretised into a rectangular grid with blocks of constant resistivity. The Helmholtz equation is translated into a difference equation for each node. Special finite domain-integral and asymptotic-boundary conditions are designed to restrict the large extent of the study domain (Weaver 1994). The asymptotic boundary conditions account for the asymptotic behavior of the field and restrict the horizontal extent of the grid. The integral boundary conditions restrict the vertical extent of the grid by transferring the integrated effect of overlying/underlying half-space to the respective horizontal boundary. These boundary conditions result in grid economy but perturb the sparse structure of typical pentadiagonal 2D FDM coefficient matrix which gets transformed to a block tridiagonal one. The boundary conditions are used to set up the algebraic equations for internal nodes. The resulting matrix equation has been solved for unknown field values using the Gaussian elimination type matrix solver that exploits the special structure of the coefficient matrix.

The ill posed inverse problem is solved using Bi-Conjugate Gradient Method (BCGM), a semi iterative

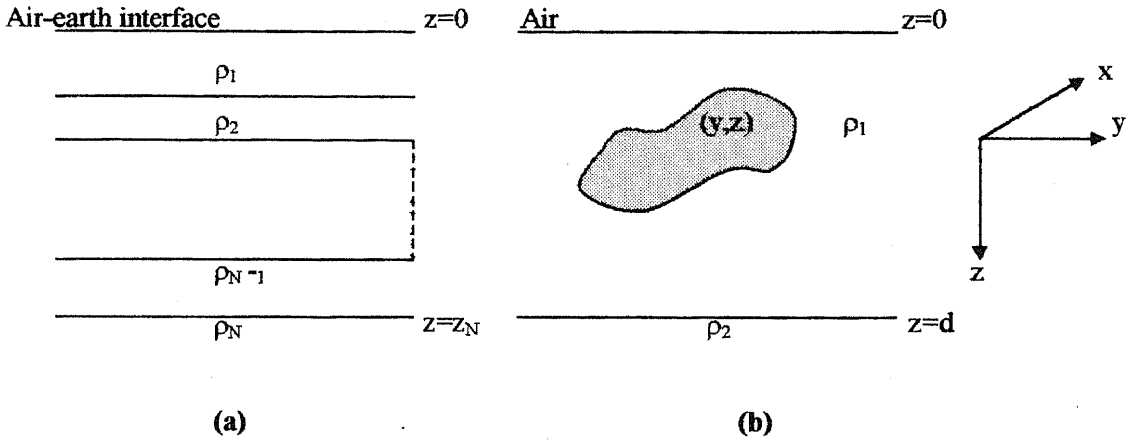

Figure 1. Schematic earth models (a) 1D and (b) 2D and Cartesian co-ordinate system.

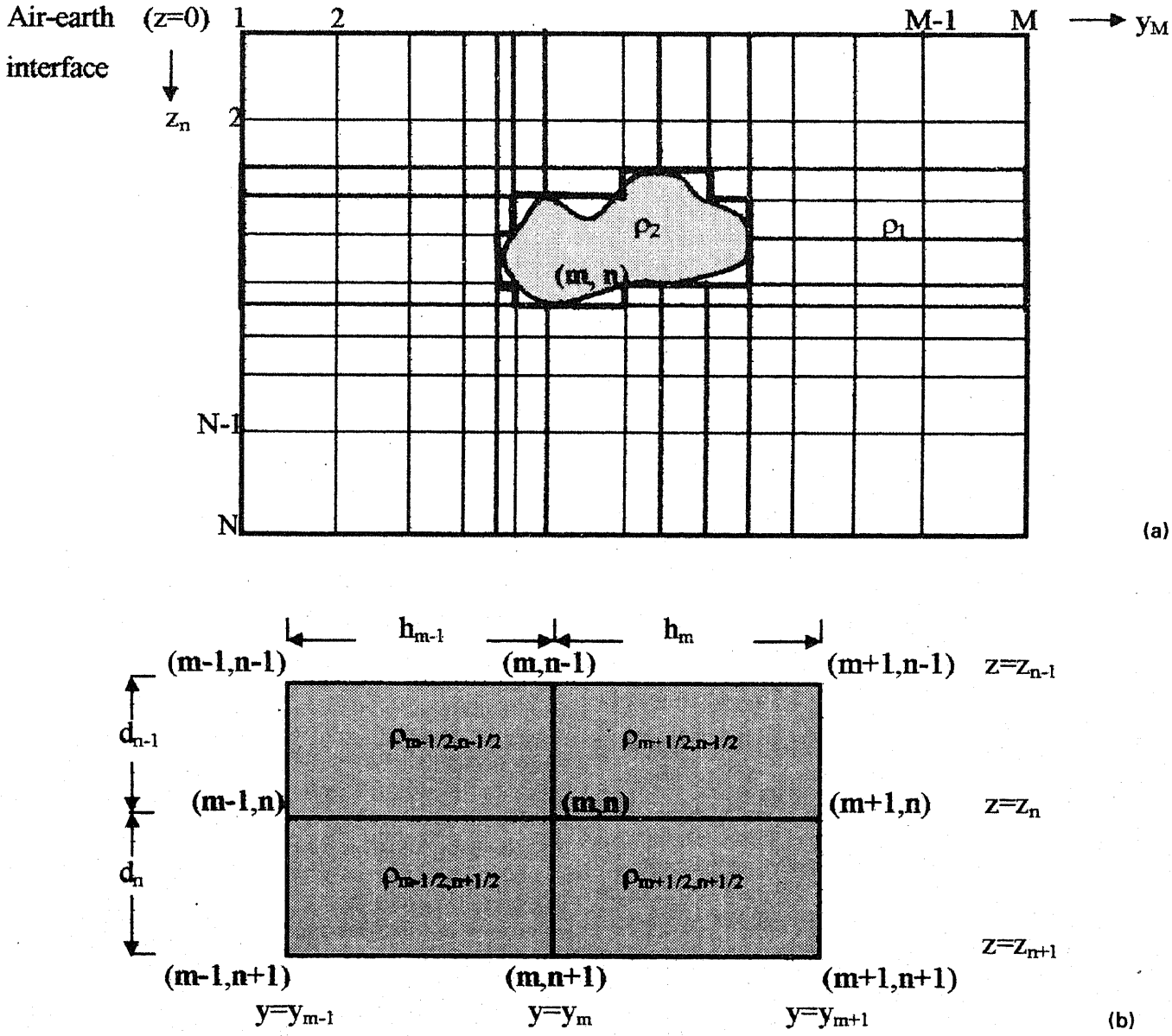

Figure 2(a). A typical finite difference grid. (b) The parameters of the four blocks surrounding the node (m, n) in 2D finite difference grid.

matrix solver (Jacobs 1986; Sarkar 1991). It dispenses with the necessity of explicit computation of the Jacobian matrix. For each BCGM iteration, the forward matrix equation is solved twice with new right hand sides, it would score over direct matrix solver as long as the number of iterations needed for the convergence of BCGM is less than half the number of blocks in the inversion domain. In order to fix the number of unknown block resistivities for all frequencies and throughout the inversion process, a super-block notion has been developed. To ensure a positive resistivity value, the logarithm of resistivity has been used. Being an iterative scheme EM2INV needs an educated guess of the model parameters to start the inversion process. The closer this initial guess is to the true model, faster is the convergence.

2.1 *EM Forward problem*

A knowledge of EM theory based on Maxwell's equations (Nabighian 1988) is essential for solving the forward problem. EM fields of an induction problem can be partitioned, depending upon the direction of the electric and magnetic fields, into two modes of polarization-Transverse Electric (TE) or E-polarization and Transverse Magnetic or B-polarization. The EM wave being a transverse wave, the vertically propagating wave fields have no vertical component in either of the above modes. For 2D modelling, the model parameters, the field vectors and the source characteristics are chosen independent of the horizontal co-ordinate x-corresponding to the strike direction. The non-vanishing magnetic field component in B-polarization and the electric field component in the E-polarization, are parallel to the strike of the 2D structure (figure 1). The set of field components of the E- and B-polarizations are distinct and independent.

The x-component of the magnetic and electric fields in the two polarizations, respectively satisfy the following partial differential equations:

$$[L_1(k)]B_x = \left[\frac{\partial^2}{\partial y^2} + \frac{\partial^2}{\partial z^2} - \frac{1}{\sigma}\frac{\partial \sigma}{\partial y} - \frac{1}{\sigma}\frac{\partial \sigma}{\partial z}\frac{\partial}{\partial z} + k^2\right]B_x = 0 \tag{1}$$

and

$$[L_2(k)]E_x = \left[\frac{\partial^2}{\partial y^2} + \frac{\partial^2}{\partial z^2} + k^2\right]E_x = 0 \tag{2}$$

where k is the wave number given by

$$k = \sqrt{-i\omega\mu\sigma} = \frac{1+i}{\delta} \quad \text{with skin depth}$$

$$\delta = \sqrt{\frac{2}{\omega\mu\sigma}}, \quad i = \sqrt{-1}$$

for frequency ω, magnetic permeability μ and conductivity σ.

In numerical methods, apart from the interface boundary conditions, certain domain boundary conditions – Dirichlet, Neumann or Mixed one – are also applied. The boundary conditions are imposed on all the four sides of the domain. For B-polarization, the magnetic field is already known at the air-earth interface. In E-polarization, to account for slow attenuation of anomalous field in the air, a thick sub-region must be introduced above the earth's surface. We have applied the integral boundary condition (Weaver 1994) for horizontal boundaries and the asymptotic boundary condition (Weaver and Brewitt-Taylor 1978) for vertical boundaries (Rastogi 1997). The partial differential equation (1) or (2) together with the integral and asymptotic boundary conditions define the complete EM boundary value problem.

In FDM, the domain of study is discretised in yz-plane by laying a grid with the help of horizontal lines, $z = z_n$ $(n = 1, 2, \ldots, N)$, and the vertical lines $y = y_m$ $(m = 1, 2, \ldots, M)$ intersecting at nodes (m, n). Here M and N are the number of vertical and horizontal grid lines respectively (figure 2(a)). Proper care should be taken while discretizing in the neighbourhood of discontinuities. Whereas, the step size can be coarse within a homogeneous region, it should be fine near the discontinuity. The cell's resistivity (or conductivity) is defined at the centre of the cell as $\rho_{m+1/2,n+1/2}$. A typical node of 2D grid with its four neighboring cells is shown in figure 2(b). The top boundary of the grid is chosen as the air-earth interface at $z = z_1 = 0$ while the bottom boundary is at $z = z_N$, a minimal vertical level in the underlying half space. The side boundaries of the grid are defined by the lines $y = y_1$ and $y = y_M$, on the left and right hand sides of the model. The variable nodal spacings, in positive y- and z-directions, are given by

$$h_m = y_{m+1} - y_m, \quad d_n = z_{n+1} - z_n,$$

where

$$1 \le m \le M-1, 1 \le n \le N-1.$$

The magnetic or electric field component at an internal node is evaluated through the respective Helmholtz equation given by equation (1) or (2). To obtain the equivalent finite difference equations, the basic step is to identify the resistivity (or conductivity) value to be assigned to a node surrounded by regions of different resistivities. A linear variation is assumed and the weighted average of resistivities (conductivity) is assigned as the resistivity (conductivity) value at the node (Weaver 1994). The discrete forms of these equations are distinct for the two modes of polarization. In order to describe these properly, the following constants are defined.

$$h_m^+ = h_m + h_{m-1};\ d_n^+ = d_n + d_{n-1};$$

$$h_m^- = h_m - h_{m-1};\ d_n^- = d_n - d_{n-1};\ h_m^p = h_m h_{m-1};$$

$$d_n^p = d_n d_{n-1};\ h_m^q = h_m h_m^+;\ d_n^q = d_n d_n^+;$$
$$h_m^r = h_{m-1} h_m^+;\ d_n^r = d_{n-1} d_n^+. \quad (3)$$

2.1.1 *B – Polarization*

The resistivity at node (m, n) is defined to be the weighted average of resistivities of the four cells surrounding it, with cell areas being the weights, as

$$\rho_{m,n} = \frac{\beta_{m,n} + \beta_{m,n-1} + \beta_{m-1,n} + \beta_{m-1,n-1}}{h_m^+ d_n^+} \quad (4)$$

where

$$\beta_{m,n} = h_m d_n \rho_{m+1/2,n+1/2}.$$

The derivatives of resistivity in the y- and z-directions are respectively defined as

$$\frac{\partial \rho}{\partial y} = \dot{\rho}_{m,n} = \frac{\rho_{m+1/2,n} - \rho_{m-1/2,n}}{h_m^+/2} \quad (5)$$

$$\frac{\partial \rho}{\partial z} = \rho'_{m,n} = \frac{\rho_{m,n+1/2} - \rho_{m,n-1/2}}{d_n^+/2}. \quad (6)$$

At the top and bottom boundaries, it is assumed that

$$\rho_{m,1} = \rho_{m,3/2},\quad \rho_{m,N} = \rho_{m,N-1/2} \quad \text{and}$$
$$\rho'_{m,1} = \rho'_{m,N} = 0. \quad (7)$$

On approximating the derivatives at the internal node (m, n) by differences, equation (1) can be written in the discrete form after some algebra as

$$\frac{2\rho_{m,n} + h_{m-1}\dot{\rho}_{m,n}}{h_m^q} B_{m+1,n} + \frac{2\rho_{m,n} - h_m \dot{\rho}_{m,n}}{h_m^r} B_{m-1,n}$$
$$+ \frac{2\rho_{m,n} + d_{n-1}\rho'_{m,n}}{d_n^q} B_{m,n+1} + \frac{2\rho_{m,n} - d_n \rho'_{m,n}}{d_n^r} B_{m,n-1}$$
$$= \left(\frac{2\rho_{m,n} - h_m^- \dot{\rho}_{m,n}}{h_m^p} + \frac{2\rho_{m,n} - d_n^- \rho'_{m,n}}{d_n^p} + i\omega\mu \right)$$
$$\times B_{m,n},\ 2 \le m \le M-1,\ 2 \le n \le N-1. \quad (8)$$

These $(M-2)(N-2)$ internal node equations provide the coefficient matrix for the evaluation of magnetic field at internal nodes.

2.1.2 *E-Polarization*

Analogous to the definition of resistivity at a node in B-polarization, for E-polarization the weighted average of conductivity at node (m, n) is defined as

$$\sigma_{m,n} = \frac{\zeta_{m,n} + \zeta_{m,n-1} + \zeta_{m-1,n} + \zeta_{m-1,n-1}}{h_m^+ d_n^+} \quad (9)$$

where, $\zeta_{m,n} = h_m d_n \sigma_{m+1/2,n+1/2}$. The equation (2) can be written in discrete form as

$$\frac{E_{m+1,n}}{h_m^q} + \frac{E_{m-1,n}}{h_m^r} + \frac{E_{m,n+1}}{d_n^q} + \frac{E_{m,n-1}}{d_n^r}$$
$$= \left(\frac{1}{h_m^p} + \frac{1}{d_n^p} + \frac{1}{2} i\alpha_{m,n}^2 \right) E_{m,n} \quad (10)$$

where, $\alpha^2 = \omega\mu\sigma$. Once the discrete governing equations are derived the supplementary discrete boundary condition equations are to be obtained next.

2.1.3 *Asymptotic boundary conditions*

For B-polarization, the magnetic field is constant at the surface. Further, within earth the anomalous field decays exponentially as $y \to \pm\infty$. As a result, the field is 1D at the side boundary nodes, i.e.

$$B_{m,1} = B_0, B_{1,n} = B_-(z_n),\quad B_{M,n} = B_+(z_n),$$
$$1 \le m \le M,\quad 2 \le n \le N \quad (11)$$

where, $B_-(z_n)$ and $B_+(z_n)$ are 1-D magnetic fields at the left and right vertical boundaries respectively.

For E-polarization the field at the left and right boundary nodes respectively are

$$E_{1,n} = E_{1,1} \left[\frac{E_-(z_n)}{E_-(0)} \right] \quad (12)$$

and

$$E_{M,n} = E_{M,1} \left[\frac{E_+(z_n)}{E_+(0)} \right] \quad (13)$$

for $2 \le n \le N$. Here, $E_-(z_n)$ and $E_+(z_n)$ are 1D electric fields at the left and right vertical boundaries. For the top nodes on the side boundaries, the FDM implementation led to the following expressions for the first and Mth node respectively (Weaver 1994).

$$(1 - \varepsilon_1) E_{1,1} - E_{2,1} = -\varepsilon_1 E_-(0) \quad (14)$$

where,

$$\varepsilon_1 = \frac{h_1(y_1 - 2h_1)}{y_1(y_1 - h_1)}$$

and

$$E_{M-1,1} - (1 + \varepsilon_M) E_{M,1} = -\varepsilon_M E_+(0) \quad (15)$$

where,

$$\varepsilon_M = \frac{h_{M-1}(y_M + 2h_{M-1})}{y_M(y_M + h_{M-1})}.$$

Equations (14) and (15) replace the infinite domain Dirichlet boundary conditions:

$$E_1 = E_-(0) \quad \text{and} \quad E_M = E_+(0) \quad (16)$$

2.1.4 *Integral boundary conditions*

For B-polarization, using the difference formula for derivatives and the 1D values at the side boundary nodes, the discrete form of the boundary conditions can be written as

$$\left[\tilde{D}_m^P + \frac{\pi\sigma_1 d_{N-1}}{h_m^r} \left(\rho_{m,N} - \frac{1}{2} h_m \dot{\rho}_{m,N} \right) \right] B_{m-1,N}$$
$$+ \left(\sum_{j=2}^{m-2} + \sum_{j=m+2}^{M-1} \right) (\tilde{W}^P)_m^j B_{j,N}$$

$$+\left[\tilde{F}_m^P+\frac{\pi\sigma_1 d_{N-1}}{h_m^q}\left(\rho_{m,N}+\frac{1}{2}h_{m-1}\dot{\rho}_{m,N}\right)\right]B_{m+1,N}$$
$$+\left[\tilde{M}_m^P-\pi\sigma_1\left(\frac{\rho_{m,N}}{d_{N-1}}+\frac{d_{N-1}}{h_m^p}\right.\right.$$
$$\left.\left.\times\left(\rho_{m,N}-\frac{1}{2}h_m\dot{\rho}_{m,N}\right)+\frac{i\omega\mu d_{N-1}}{2}\right)\right]B_{m,N}$$
$$=[(N_f^P)_m^1-Q_m^1]B_-(z_n)+[(N_f^P)_m^M-Q_m^M]B_+(z_n),$$
$$2\le m\le M-1. \quad (17)$$

The coefficients Q_m^1 and Q_m^M are given by equations (5.21) – (5.22) of Weaver (1994, p. 164) while other coefficients $D_m^P, W_m^P, F_m^P, M_m^P$ and N_f^P are given by equations (5.84) – (5.90) of Weaver (1994, p. 175) with his constant B_m^P replaced by W_m^P here. The boundary condition represented by equations (11) and the $(M\text{-}2)$ equations (17) along with the $(M\text{-}2)(N\text{-}2)$ internal node equations (8), complete the linear system of equations to be solved for the $(M\text{-}2)(N\text{-}1)$ unknowns $B_{m,n}$.

In E-polarization, the Neumann integral boundary conditions are applied on the top as well as the bottom boundary interfaces. On substituting the difference formula and using asymptotic boundary condition, the top boundary condition can be stated in the following discrete form:

$$\tilde{P}_m^1E_{1,1}+\tilde{P}_m^ME_{M,1}+\left(\frac{\pi d_1}{h_m^r}+C_m\right)E_{m-1,1}$$
$$+\left(\frac{\pi d_1}{h_m^q}+U_m\right)E_{m+1,1}+\left(\sum_{j=2}^{m-2}+\sum_{j=m+2}^{M-1}\right)A_m^jE_{j,1}$$
$$+\left(L_m-\frac{\pi}{d_1}-\frac{\pi d_1}{h_m^p}-\frac{\pi i d_1\alpha_{m,1}^2}{2}\right)E_{m,1}$$
$$+\frac{\pi}{d_1}E_{m,2}=R_m^1E_-(0)+R_m^ME_+(0)-\pi i\omega B_0,$$
$$2\le m\le M-1. \quad (18)$$

On the other hand, the discrete form of bottom boundary condition is

$$\tilde{Q}_m^1E_{1,N}+\tilde{Q}_m^ME_{M,N}+\left(\frac{\pi d_{N-1}}{h_m^r}+\tilde{D}_m\right)E_{m-1,N}$$
$$+\left(\frac{\pi d_{N-1}}{h_m^q}+\tilde{F}_m\right)E_{m+1,N}+\left(\sum_{j=2}^{m-2}+\sum_{j=m+2}^{M-1}\right)B_m^jE_{j,N}$$
$$+\left(\tilde{M}_m-\frac{\pi}{d_{N-1}}-\frac{\pi d_{N-1}}{h_m^p}-\frac{\pi i d_{N-1}\alpha_{m,N}^2}{2}\right)E_{m,N}$$
$$+\frac{\pi}{d_{N-1}}E_{m,N-1}=\tilde{S}_m^1E_-(z_n)+\tilde{S}_m^ME_+(z_n),$$
$$2\le m\le M-1. \quad (19)$$

The coefficients in equations (18) and (19) are defined in equations (5.11) – (5.18), (5.50) – (5.66) and (5.87) – (5.91) of Weaver (1994, p. 163–164, 169–170, 175) with his constant U^M replaced by E^M here. The $(2N\text{-}2)$ asymptotic boundary condition equations (12) and (13), equations (14) and (15) on the top corner nodes, $(2M\text{-}4)$ equations (18) and (19) for the top and bottom interfaces, complete the boundary condition equations. These, together with the $(M\text{-}2)(N\text{-}2)$ internal node equations (8) and (10), give a total of MN equations in $E_{m,n}$ unknowns.

The linear system of equations for both modes of polarization can be compiled and written in a matrix form as

$$\mathbf{CF}=\mathbf{S}. \quad (20)$$

$\mathbf{C}$ is the coefficient matrix comprising the terms from equation (8) and (17) or (10), (18) and (19), $\mathbf{S}$ is the known vector derived from boundary conditions and $\mathbf{F}$ is the unknown magnetic or electric field component vector. The size of the coefficient matrix is $n_t\times n_t$ where n_t, the number of unknowns, is

$$n_t=\begin{cases}n_i+(M\text{-}2) & \text{for B-polarization}\\ n_i+2(M\text{-}2) & \text{for E-polarization}\end{cases}$$

with $n_i=(M\text{-}2)\times(N\text{-}2)$, being the number of internal nodes.

The matrix $\mathbf{C}$ would look like

$$\begin{bmatrix}\mathbf{M}_1 & \mathbf{M}_2 & 0\\ \mathbf{M}_3 & \mathbf{M}_4 & \mathbf{M}_5\\ 0 & \mathbf{M}_6 & \mathbf{M}_7\end{bmatrix}$$

with $\mathbf{M}_1$ and $\mathbf{M}_7$ being full submatrices, $\mathbf{M}_2, \mathbf{M}_3, \mathbf{M}_5$ and $\mathbf{M}_6$ being diagonal matrices and $\mathbf{M}_4$ being a tri-diagonal matrix. The elements of matrix $\mathbf{C}$ are different for E- and B-polarization. For B-polarization, the pth row for internal nodes of the coefficient matrix $\mathbf{C}$ has the following five non zero elements

$$C_{p,q1}=(h_{p-1}\rho_{p-1,q3-1}+h_p\rho_{p,q3-1})/d_{q3-1},$$
$$C_{p,q2}=(d_{q3}\rho_{p-1,q3}+d_{q3-1}\rho_{p-1,q3-1})/h_{p-1},$$
$$C_{p,q3}=(C_{p,q1}+C_{p,q2}+C_{p,q4}+C_{p,q5})+\frac{1}{2}\omega\mu h_p^+d_{q3}^+,$$
$$C_{p,q4}=(d_{q3-1}\rho_{p,q3-1}+d_{q3}\rho_{p,q3})/h_p, \quad (20a)$$
$$C_{p,q5}=(h_p\rho_{p,q3-1}+h_{p-1}\rho_{p-1,q3})/d_{q3};$$
$$h_p^+=h_p+h_{p-1}, d_{q3}^+=d_{q3}+d_{q3-1}.$$

The column numbers q's are given as

$$q1=p-M+2,\ q2=p-1,\ q3=p,\ q4=p+1,$$
$$q5=p+M-2. \quad (20b)$$

Similarly, for E-polarization, the five nonzero elements of pth row can be written as

$$C_{p,q1}=h_p^+/d_{q3-1},$$
$$C_{p,q2}=d_{q3}^+/h_{p-1},$$
$$C_{p,q3}=\left[\frac{h_p^+}{d_{q3-1}}+\frac{h_p^+}{d_{q3}}+\frac{d_{q3}^+}{h_p}+\frac{d_{q3}^+}{h_{p-1}}+\frac{1}{2}\omega\mu\right.$$
$$\times(h_{p-1}d_{q3-1}\sigma_{p-1,q3-1}+h_{p-1}d_{q3}\sigma_{p-1,q3}$$
$$\left.+h_pd_{q3-1}\sigma_{p,q3-1}+h_pd_{q3}\sigma_{p,q3})\right],$$

$$C_{p,q4} = d^+_{q3}/h_p,$$
$$C_{p,q5} = h^+_p/d_{q3},$$

and the column number q's are given by the same equation (20b). Once the main field component, $\mathbf{B}_x$ or $\mathbf{E}_x$ is computed, the other field components can be derived from it through the requisite transformation matrices.

For B-polarization, only the horizontal component of the electric field, $\mathbf{E}_y$ is of practical interest that can be derived as

$$\mathbf{E}_y = (\mathbf{T}^B_y)\mathbf{B} \tag{21}$$

where, $\mathbf{T}^B_y$ is the transformation matrix of order $(M\text{-}2)\times n_t$. The nonzero elements of its pth row are

$$(\mathbf{T}^B_y)_{p,q3} = \omega\frac{r_{p1q}}{h_{p-1}}\left[-\frac{1}{d_1^2} - \frac{i}{2}d_1\frac{h^+_p}{r_{pq}+r_{p1q}}\right],$$
$$(\mathbf{T}^B_y)_{p,q5} = \omega\frac{r_{p1q}}{h_{p-1}}\frac{1}{d_1^2},$$
$$r_{p,q} = h_p d_1\frac{\rho_{p,1}}{\omega}\mu; \quad r_{p1q} = h_{p-1}d_1\frac{\rho_{p-1,1}}{\omega}\mu.$$

Once $\mathbf{E}_y$ is evaluated the impedance $\mathbf{Z}_{yx}$ can be computed as

$$\mathbf{Z}_{yx} = (\mathbf{T}_{yx})\mathbf{B}, \quad \mathbf{T}_{yx} = [\mathbf{D}_{B_x}]^{-1}\mathbf{T}^B_y \tag{22}$$

where, $\mathbf{D}_{B_x}$ is the diagonal matrix whose elements comprises the B_x values.

Similarly, for E-polarization, the horizontal and vertical components of the magnetic field, $\mathbf{B}_y$ and $\mathbf{B}_z$ can also be derived. These field components, the impedance $\mathbf{Z}_{xy}$ and the induction vector $\mathbf{I}_{yz}$ can be written in the matrix notation as

$$\begin{aligned}\mathbf{B}_y &= \mathbf{T}^E_y\mathbf{E},\\ \mathbf{B}_z &= \mathbf{T}^E_z\mathbf{E},\\ \mathbf{Z}_{xy} &= \mathbf{T}_{xy}\mathbf{E},\\ \mathbf{I}_{zy} &= \mathbf{T}_{zy}\mathbf{E}\end{aligned} \tag{23}$$

where, $\mathbf{T}^E_y, \mathbf{T}^E_z, \mathbf{T}_{xy}$ and $\mathbf{T}_{zy}$are the $(M\text{-}2)\times n_t$ transformation matrices. The nonzero elements of the pth row of different matrices are

$$(\mathbf{T}^E_y)_{p,q1} = \frac{i}{\omega}\frac{d_1}{h^r_p},$$
$$(\mathbf{T}^E_y)_{p,q3} = \frac{1}{2}\mu d_1\frac{(h_p/\rho_{p,1}+h_{p-1}/\rho_{p-1,1})}{h^+_p} - \frac{i}{\omega}\frac{d_1}{h^p_p} - \frac{i}{\omega}\frac{1}{d_1},$$
$$(\mathbf{T}^E_y)_{p,q4} = \frac{i}{\omega}\frac{d_1}{h^q_p},$$
$$(\mathbf{T}^E_y)_{p,q5} = \frac{i}{\omega}\frac{1}{d_1},$$
$$(\mathbf{T}^E_z)_{p,q2} = \frac{i}{\omega}\frac{h_p}{h^r_p},$$
$$(\mathbf{T}^E_z)_{p,q3} = \frac{i}{\omega}\left[\frac{h_{p-1}-h_p}{h^p_p} + \frac{i}{2}\omega\mu\left(\frac{1}{\rho_{p,1}} - \frac{1}{\rho_{p-1,1}}\right)\frac{h^p_p}{h^+_p}\right],$$
$$(\mathbf{T}^E_z)_{p,q4} = -\frac{i}{\omega}\frac{h_{p-1}}{h^q_p}.$$

The transformation matrices for impedance and induction vector are given as

$$\begin{aligned}\mathbf{T}_{xy} &= [\mathbf{D}_{B_y}]^{-1},\\ \mathbf{T}_{zy} &= [\mathbf{D}_{B_y}]^{-1}[\mathbf{T}^E_z]\end{aligned} \tag{24}$$

where, $\mathbf{D}_{B_y}$, a diagonal matrix, is comprised of $\mathbf{B}_y$ values. Thus, any field component, impedance or induction vector can be computed, using these relations and then the corresponding Jacobian can be evaluated.

2.1.5 *Forward matrix solver*

The forward matrix equation has been solved using the Gaussian elimination, a direct method. Special measures are taken to exploit the special block tridiagonal structure of the coefficient matrix. The FDM coefficient matrix $\mathbf{C}$ is complex and has distributed eigenvalues. To exploit its special sparsity structure, iterative methods can be used. The early workers (Jones and Pascoe 1972; Hibbs and Jones 1976) did use relaxation methods but they did not address, in detail, its accuracy. Apart from this, though the matrix is diagonally dominant, yet the off-diagonal elements, corresponding to the second and $(M\text{-}1)$th nodes, are almost equal to the diagonal one restricting the use of iterative methods. Moreover, for the solution of a matrix equation with different right hand sides, the direct methods may score over iterative ones inspite of the enormous sparsity of the coefficient matrix.

Another alternative is to use the conjugate gradient (CG) method that is a semi-iterative method. Due to distributed eigenvalues of the matrix $\mathbf{C}$, it will result in a number of iterations approaching the order of matrix. Although the number of CG iterations is less than what is needed in iterative methods, the time taken may, in some cases, equal that for the iterative method because of the complexity of a CG iteration. To overcome this inefficiency, preconditioning, an algebraic procedure to generate a transformed system of equations having a better eigenvalue spectrum, is used (Jacobs 1981). The widely used preconditioner, the complete Cholesky decomposition (Meijerink and van der Vorst 1977; Kershaw 1978), works satisfactorily only for a real and positive definite matrix. Another possible approach is to use augmented conjugate algorithm where the original complex system is augmented by its adjoint (Sarker *et al* 1988). But since the positive definiteness of the matrix is not known *a priori*, it can not be used. Mackie and Madden (1993) and Mackie *et al* (1994) have used a minimum residual algorithm for real symmetric matrices (Axxelson 1980) by neglecting the imaginary part of the diagonal term. This approach could not be followed as the coefficient matrix $\mathbf{C}$ is not symmetric.

In the case of matrix solvers based on direct methods, the already existing LU decomposition of matrix $\mathbf{C}$ can be reused. In other methods, the whole procedure is to be done afresh each time. All these points justified the use of the direct method for solving the forward problem.

2.2 *The Inverse problem*

The 2D non-linear inverse problem is posed by quasi-linearizing the Taylor series of the response function $F_i(P_j)$ about an initial guess parameter vector $\mathbf{P}^0$ as

$$F_i(P_j) = F_i(P_j^0) + \sum_{j=1}^{n} \frac{\partial F_i}{\partial P_j}(P_j - P_j^0) + \frac{1}{2}\sum_{j=1}^{n}\sum_{k=1}^{n} \times \frac{\partial^2 F_i}{\partial P_j \partial P_k}(P_j - P_j^0)(P_k - P_k^0) + \cdots \quad j = 1, 2, \ldots, m. \tag{25}$$

This equation can be written in a concise form with $\mathbf{J}$ and $\mathbf{H}$ as the Jacobian and Hessian matrices respectively as

$$\mathbf{F}(\mathbf{P}) = \mathbf{F}(\mathbf{P}^0) + \mathbf{J}\Delta\mathbf{P} + \tfrac{1}{2}\Delta\mathbf{P}^T\mathbf{H}\Delta\mathbf{P} + \cdots$$

that reduces to the following simple form if $\mathbf{P}^0$ is sufficiently close to $\mathbf{P}$

$$\Delta\mathbf{R} = \mathbf{J}\Delta\mathbf{P} \tag{26}$$

where $\Delta\mathbf{R}$ is the difference column vector between the observed and computed responses $\mathbf{F}(\mathbf{P})$ and $\mathbf{F}(\mathbf{P}^0)$ respectively, $\Delta\mathbf{P}$ is the unknown parameter correction column vector and $\mathbf{J}$ is the Jacobian matrix comprising partial derivatives of observed response function (data) with respect to the unknown parameters. The matrix $\mathbf{J}$ is a measure of how each data point would be affected by a change in a particular parameter and is normally termed as 'sensitivity matrix'. The inverse solution of equation (26) is obtained using the ridge-regression least squares and ridge-regression minimum norm estimator as

$$\Delta\hat{\mathbf{P}} = (\mathbf{J}^H\mathbf{J} + \lambda^2\mathbf{I})^{-1}\mathbf{J}^H\Delta\mathbf{R} \tag{27}$$

and,

$$\Delta\hat{\mathbf{P}} = \mathbf{J}^H(\mathbf{J}\mathbf{J}^H + \lambda^2\mathbf{I})^{-1}\Delta\mathbf{R} \tag{28}$$

respectively. The solution of equation (26) in current iteration is used to update the initial guess to be used for the next iteration as

$$\mathbf{P} = \mathbf{P}^0 + \Delta\hat{\mathbf{P}}. \tag{28a}$$

At the end of each individual iteration, the inverse solution is checked for convergence. The inversion process is stopped the moment either the convergence is achieved or the iteration number exceeds the specified limit.

From the inverse problem formulation it is evident that the basic steps of every inversion iterations are the forward computation, the generation of Jacobian matrix and finally the solution of equation (26). Therefore saving at any of these steps can significantly reduce the total computer time. The Jacobian matrix in equation (26) is composed by differentiating equation (20) with respect to the unknown resistivity parameter, P_j,

$$\mathbf{C}\frac{\partial\mathbf{F}}{\partial P_j} + \frac{\partial\mathbf{C}}{\partial P_j}\mathbf{F} = 0 \quad j = 1, 2, \ldots, m. \tag{29}$$

This can be cast into the following matrix equation

$$\mathbf{C}\mathbf{J} = \mathbf{Y} \tag{30}$$

where, the jth columns of matrices $\mathbf{J}$ and $\mathbf{Y}$ are

$$\mathbf{J}_j = \frac{\partial\mathbf{F}}{\partial P_j} \quad \text{and} \quad \mathbf{Y}_j = \frac{\partial\mathbf{C}}{\partial P_j}\mathbf{F}.$$

It should be mentioned here that the initial guess is the current estimate of ρ_j, the resistivity of the jth block. For numerical accuracy, $\log\rho_j$ is used as a parameter vector

$$P_j = \log\rho_j = -\log\sigma_j. \tag{30a}$$

The derivative with respect to it is defined as

$$\frac{\partial}{\partial P_j} = \frac{1}{\rho_j}\frac{\partial}{\partial\rho_j} = -\frac{1}{\sigma_j}\frac{\partial}{\partial\sigma_j}.$$

Equations (20) and (30) have the same coefficient matrix $\mathbf{C}$. Therefore, in the case of a matrix solver based on direct methods, the already existing Lower and Upper triangular (LU) decomposition of it can be reused. Thus, each column of the matrix $\mathbf{J}$ can be efficiently computed using equation (20) with the corresponding columns of matrix $\mathbf{Y}$ as a new right hand side. After composing the matrix $\mathbf{J}$, the estimation given by equation (27) or (28) is used for obtaining the inverse solution. For every inversion iteration equation (26) is solved as many times as the number of unknown resistivity parameters. The Jacobian for the various response functions can be derived from the following expression of the derived response functions

$$\mathbf{R} = \mathbf{T}\mathbf{F} \tag{31}$$

with $\mathbf{R}$ as the derived response function vector, $\mathbf{T}$ as the transformation matrix formed from the relationship between the response function and the respective field components and $\mathbf{F}$ as the corresponding field component vector. Differentiating (31) with respect to P_j, we get

$$\frac{\partial\mathbf{R}}{\partial P_j} = \mathbf{T}\frac{\partial\mathbf{F}}{\partial P_j} + \frac{\partial\mathbf{T}}{\partial P_j}\mathbf{F}. \tag{32}$$

2.2.1 *Derivative of coefficient matrix*

The derivative of a coefficient matrix element is zero unless its expression contains ρ_j. Since an internal node is associated with four regions, the elements of the row corresponding to this node contain only these

four block resistivities. As a result, the matrix $\mathbf{J}$ is grossly sparse with each row having at most four non-zero entries in column positions corresponding to the element whose resistivity is perturbed. For B-polarization, the derivatives of different entries in the pth row of matrix $\mathbf{C}$ are:

$$\begin{aligned}
\frac{\partial C_{p,q1}}{\partial P_j} &= -\left(\frac{h_p^+}{d_{q1-1}}\right)\frac{1}{P_j},\\
\frac{\partial C_{p,q3}}{\partial P_j} &= -(C_{p,q1}+C_{p,q2}+C_{p,q4}+C_{p,q5})\frac{1}{P_j},\\
\frac{\partial C_{p,q4}}{\partial P_j} &= -\left(\frac{h_p^+}{d_{q4}}\right)\frac{1}{P_j},\\
\frac{\partial C_{p,q5}}{\partial P_j} &= -\left(\frac{d_{q5}^+}{h_{p-1}}\right)\frac{1}{P_j},
\end{aligned} \tag{33}$$

where q_j's are given by equation (20b).

For E-polarization, since the resistivity appears only in the imaginary term of the diagonal element, all the off diagonal terms will vanish. The pth diagonal element of derivative matrix is

$$\frac{\partial C_{p,q3}}{\partial P_j} = -i\omega\frac{\mu}{2}h_{p-1}d_{q3-1}\frac{1}{P_j}. \tag{34}$$

If the body is outcropping, in E-polarization, the top row block matrix, corresponding to the top integral boundary condition is to be differentiated with respect to P_j. Since only the node at which the condition is being evaluated contains a resistivity term, all other entries in the full block will vanish. The derivative of the diagonal element of the top block is given by

$$\frac{\partial C_{p,q3}}{\partial P_j} = i\omega\frac{\pi\mu}{2}d_{q3}\frac{h_{p-1}}{h_p}\frac{1}{P_j}. \tag{35}$$

Once, computation of the derivative of the coefficient matrix $\mathbf{C}$ is over, it is multiplied with the corresponding field vector $\mathbf{F}$ to construct the jth column of the right hand side matrix $\mathbf{Y}$ of equation (30).

2.2.2 *Computation of Jacobian/derived Jacobians*

The Jacobian matrix $\mathbf{J}$ can be computed explicitly by solving equation (26) using any standard matrix solver. The Jacobian $\mathbf{J}_x^{E,B}$, corresponding to the main field component, $\mathbf{B}_x$ or $\mathbf{E}_x$, is used to derive the Jacobians for derived response functions.

For B-polarization, the jth column of Jacobian, $\mathbf{J}_{yx}$, of impedance $\mathbf{Z}_{yx}$ can be written as

$$\frac{\partial \mathbf{Z}_{yx}}{\partial P_j} = (\mathbf{J}_{yx})_j = [\mathbf{D}_{B_x}]^{-1}\frac{\partial \mathbf{E}_y}{\partial P_j} - [\mathbf{D}_{E_y}][\mathbf{D}_{B_x}]^{-2}\frac{\partial \mathbf{B}_x}{\partial P_j} \tag{36}$$

where, $\mathbf{D}_{B_x}$ and $\mathbf{D}_{E_y}$ are the diagonal matrices for $\mathbf{B}_x$ and $\mathbf{E}_y$ respectively. From equation (23), since the constant magnetic field does not depend on resistivity, the second term will vanish and the above equation will reduce to the following equation

$$(\mathbf{J}_{yx})_j = [\mathbf{D}_{B_x}]^{-1}\left[\mathbf{T}_y\frac{\partial \mathbf{B}_x}{\partial P_j} + \frac{\partial \mathbf{T}_y}{\partial P_j}\mathbf{B}_x\right]. \tag{37}$$

For E-polarization, the Jacobians $\mathbf{J}_{xy}$ for the impedance $\mathbf{Z}_{xy}$ can be derived as

$$\frac{\partial \mathbf{Z}_{xy}}{\partial P_j} = (\mathbf{J}_{xy})_j = [\mathbf{D}_{B_y}]^{-1}\frac{\partial \mathbf{E}_x}{\partial P_j} - [\mathbf{D}_{E_x}][\mathbf{D}_{B_y}]^{-2}\frac{\partial \mathbf{B}_y}{\partial P_j}. \tag{38}$$

On using equation (23), it reduces to the following equation

$$(\mathbf{J}_{xy})_j = [\mathbf{D}_{B_y}]^{-1}[\mathbf{J}_x^E - \mathbf{Z}_{xy}\mathbf{T}_y\mathbf{J}_x^E - \mathbf{Z}_{xy}\mathbf{T}'_y\mathbf{E}_x]. \tag{39}$$

Here $\mathbf{T}'_y$ is the derivative of transformation matrix $\mathbf{T}_y$ with respect to P_j.

For induction vector $\mathbf{I}_{zy}$, the jth column of the Jacobian $\mathbf{J}_{zy}$ can be written as

$$\frac{\partial \mathbf{I}_{zy}}{\partial P_j} = (\mathbf{J}_{zy})_j = [\mathbf{D}_{B_y}]^{-1}\frac{\partial \mathbf{B}_z}{\partial P_j} - [\mathbf{D}_{\mathbf{B}_z}][\mathbf{D}_{B_y}]^{-2}\frac{\partial \mathbf{B}_y}{\partial P_j}. \tag{40}$$

Using the respective transformation matrices from equation (23), the above equation reduces to the following form

$$(\mathbf{J}_{zy})_j = [\mathbf{D}_{B_y}]^{-1}[(\mathbf{T}_z - \mathbf{I}_{zy}\mathbf{T}_y)\mathbf{J}_x^E + (\mathbf{T}'_z - \mathbf{I}_{zy}\mathbf{T}'_y)\mathbf{E}_x] \tag{41}$$

where superscript ($'$) indicates differentiation with respect to P_j. The different forms of Jacobian matrices can be written in a generalized form as

$$\mathbf{J}_R = \mathbf{T}'\mathbf{F} + \mathbf{T}\mathbf{J}_x. \tag{42}$$

Depending upon the response vector $\Delta\mathbf{R}$, the transformation matrices are developed and the derived Jacobians are computed. Once $\mathbf{J}$ is evaluated, the inverse problem equation (26) can be solved using a suitable matrix solver.

2.2.3 *Inverse matrix solver*

The EM inverse problem is stated, in a matrix form, in equation (26). On account of the finite and erroneous data, the problem is ill-posed and needs to be regularised for obtaining an approximate solution. The problem is, in general, either overdetermined or underdetermined, depending upon the number of observations and parameters. For such cases, ridge-regressed least square or minimum norm estimators are used.

To obtain a least square or minimum norm solution, the matrix $\mathbf{J}$ should be evaluated before hand using equation (27) or equation (28). Since the inverse problem given by equation (26) is to be solved only for the single right hand side, semi-iterative methods can be used instead of the direct ones. Due to real data

being invariably erroneous, the resulting system of governing equations will be inconsistent. Therefore, only an approximate solution can be sought. This means that inaccuracy in the estimation of unknown parameters within a prescribed error range can be tolerated and this can be more efficiently achieved through iterative or semi-iterative methods. But when solved using direct or iterative methods, equation (20) is to be solved as many times as the number of blocks in the inversion domain, for each inversion iteration. In the case of CGM, on the other hand, one avoids the explicit construction of $\mathbf{J}$. Instead, only the product of $\mathbf{J}$ or of its Hermitian with a given vector need be known. It is so because the coefficient matrix appears only in the product of the search vector $\mathbf{P}$ with itself. Hence, equation (20) is to be solved only twice for every inversion iteration.

Most of the literature on CGM has only dealt with the case of a real, symmetric and positive definite matrix (Reid 1971). However, the system of equation (26) is complex. As a result, it is solved using the complex Bi-Conjugate Gradient Method (BCGM) where the matrix $\mathbf{J}$ or its Hermitian appears only in their product with the search vector $\mathbf{P}$ (Jacobs 1986). Since the resistivity is a real quantity, only the real part of the correction vector $\Delta\mathbf{P}$ is retained. The irregular behaviour of convergence is observed in BCGM. Moreover, the solution, as obtained, does not reflect the true behaviour of the resistivity. Hence, a way out has been found to recast equation (26) into real form and the regular steps of BCGM are modified to solve this equation for an equivalent real system. The complex matrix and the right hand side are broken up into their real and imaginary parts and the equation (26) is written as

$$(\mathbf{J}_r + i\mathbf{J}_i)\Delta\mathbf{P} = (\Delta\mathbf{R}_r + i\Delta\mathbf{R}_i) \tag{43}$$

where, the 'r' and 'i' subscripts denote the real and imaginary parts respectively. Equation (43) can be written as

$$\begin{pmatrix}\mathbf{J}_r\\ \mathbf{J}_i\end{pmatrix}\Delta\mathbf{P} = \begin{pmatrix}\Delta\mathbf{R}_r\\ \Delta\mathbf{R}_i\end{pmatrix}$$

or

$$\mathbf{J}_c\Delta\mathbf{P} = \Delta\mathbf{R}_c \tag{44}$$

where, the subscript 'c' indicates appended real and imaginary components of the quantity. The solution so obtained, correction vector $\Delta\mathbf{P}$, is real. There is no need of preconditioning as the system converges in two or three iterations. The inverse solution is obtained using BCGM to solve the matrix equation of type $\mathbf{Ax} = \mathbf{b}$, with the coefficient matrix $\mathbf{A}$ and the right hand side vector $\mathbf{b}$ defined for the two estimators given by equation (27) or (28).

For the least squares,

$$\mathbf{A} = (\mathbf{J}_c^T\mathbf{J}_c + \lambda^2\mathbf{I})$$

and

$$\mathbf{b} = \mathbf{J}_c^T\Delta\mathbf{R}_c.$$

For the minimum norm,

$$\mathbf{A} = (\mathbf{J}_c\mathbf{J}_c^T + \lambda^2\mathbf{I})$$

and

$$\mathbf{b} = \Delta\mathbf{R}_c.$$

For the minimum norm estimator, the solution vector $\mathbf{x}$ is multiplied by $\mathbf{J}_c^T$ to get the estimate. Hence, for solving the above equations, the product $(\mathbf{J}_c^T\mathbf{J}_c)\mathbf{q}$ or $(\mathbf{J}_c\mathbf{J}_c^T)\mathbf{q}$ is required. These can be computed as described below. Rewriting equation (26) in real and imaginary parts as:

$$(\mathbf{C}_r + i\mathbf{C}_i)(\mathbf{J}_r + i\mathbf{J}_i) = \mathbf{Y}_r + i\mathbf{Y}_i, \tag{45}$$

and splitting this into two equations corresponding to the real and imaginary parts, we get

$$\mathbf{C}_r\mathbf{J}_r - \mathbf{C}_i\mathbf{J}_i = \mathbf{Y}_r \tag{46}$$

and,

$$\mathbf{C}_i\mathbf{J}_r + \mathbf{C}_r\mathbf{J}_i = \mathbf{Y}_i. \tag{47}$$

Equation (46) and (47) can be combined as:

$$\begin{bmatrix}\mathbf{C}_r & -\mathbf{C}_i\\ \mathbf{C}_i & \mathbf{C}_r\end{bmatrix}\begin{pmatrix}\mathbf{J}_r\\ \mathbf{J}_i\end{pmatrix} = \begin{pmatrix}\mathbf{Y}_r\\ \mathbf{Y}_i\end{pmatrix}$$

or,

$$\mathbf{C}_c\mathbf{J}_c = \mathbf{Y}_c. \tag{48}$$

Multiplying equation (48) with an arbitrary vector $\mathbf{q}$ and solving we get:

$$\mathbf{J}_c\mathbf{q} = \mathbf{C}_c^{-1}\mathbf{Y}_c\mathbf{q}. \tag{49}$$

Similarly, taking transpose of equation (48), solving and then multiplying with the arbitrary vector $\mathbf{q}$ we get

$$\mathbf{J}_c^T\mathbf{q} = \mathbf{Y}_c^T(\mathbf{C}_c^T)^{-1}\mathbf{q}. \tag{50}$$

For every inversion iteration equation (20) is solved with as many right hand sides as the number of blocks in the case of direct methods while in the case of BCGM, it is solved only twice for each conjugate gradient iteration. Hence, BCGM scores over the direct method as long as the number of iterations needed for convergence is less than half the number of blocks in the inverted model. Further, BCGM is preferred to other iterative matrix solvers because of its faster convergence rate. One iteration of the quasi-linear inversion includes the solution of the forward problem, generation of Jacobian and the solution of the inverse problem. While solving the inverse problem, there are two levels of iterations. The outer loop is on the iterations of quasi-linearization and the inner loop is on the iterations of the BCGM to obtain the parameter correction vector. The correction vector $\Delta\hat{\mathbf{P}}$ obtained by solving the inverse problem is added

to the initial guess $\mathbf{P}^0$. However, since P_j is related to ρ_j through equation (30a), equation (28a) gets modified as

$$\rho_j = \rho_j^0 \exp(\Delta \hat{P}_j). \tag{51}$$

The logarithmic parameterization works well for larger changes in the model parameter resulting from larger dynamic range in the signals and therefore it stabilizes the inversion process. After each iteration the solution convergence is checked on two counts, the degree of improvement in the parameter vector and the level of fit. For the latter, the computed response of the model is compared with the observed one and the root mean square (rms) error is then compared with the pre-assigned threshold value.

3. Numerical experiments

Based on the above development, a software has been developed that consists of 6120 lines, 42 subroutines and 3 function subprograms. The main program has two basic modules-forward and inverse. It is written in FORTRAN 77 and implemented on an IBM compatible EISA based PC486 machine with 32 MB RAM and 383 MB hard disk, using SVR 4.0 version of Unix operating system and F 78 FORTRAN compiler. For a typical model with 31 × 15 nodes, the program takes about 3 min for 10 inversion iterations.

Once the software is developed, it becomes essential to establish its accuracy and efficiency. Every aspect of the algorithm EM2INV was checked by designing exercises of diverse nature. For understanding the relationship between various model parameters and the computed responses, experiments for forward algorithm have been specially devised. Results of these experiments help in setting up the guidelines that can be used for a successful inversion of real data.

3.1 *Forward algorithm*

A model solved by Brewitt-Taylor and Weaver (1976) which will henceforth be referred to as the BW model is used for these tests. The model is $500 \times 500\,\mathrm{m}^2$ square target of resistivity 0.1 ohm m, buried at a depth of 100 m, in a half-space of 1 ohm m. The Dirichlet boundary conditions are imposed at the domain boundaries and the BW grid comprises 41 × 41 nodes. Horizontally, the body is located at the centre of the grid. Real and imaginary parts of the electric field at grid points are found to be in excellent agreement with those of BW. The accuracy of finite difference method depends on grid spacing of the mesh (Chen and Fung 1989). For mesh convergence study, a comparison between various coarser and finer versions of BW grid, along with the optimal grid used by EM2INV, was made. The mesh spacings which are four and two times of the original grid spacing result in the coarser grids of 11 × 11 and 21 × 21 nodes respectively, whereas a finer 81 × 81 nodes grid is obtained when spacings are reduced by half. The size of EM2INV grid which was generated by an automatic grid generator, is 31 × 12. The real and imaginary components of the electric field for all these grids exhibit excellent convergence to those of finer grid. The refinement of optimal grid does not improve the results at all. The reduction in size of the optimal grid renders significant reduction in computation time. Another test conducted on the algorithm was to verify the convergence of the buried target response to that of a half-space when the resistivity contrast is reduced to 1. The resistivity of the rectangular target of BW model is modified to 0.9 ohm m for this test. The impedance for the E- and B-polarization were computed and found to be identical within computational errors.

A comparison of results obtained by the forward algorithm with published results was the next method of validation. For this purpose the bench mark model is taken from the report of an international project on the comparison of modelling methods for EM induction problems (Zhdanov *et al* 1990). In this report the results of important numerical methods developed by various workers through out the globe are compiled. Here we present only two models. The first model (figure 3(a)) is a two layer one with layer resistivities 100 and 10 ohm m. Two conductive blocks of resistivities 0.01 ohm m and 0.1 ohm m are embedded in the first layer at a depth of 7 km. The second model (figure 3(b)) has a 10 km thick inhomogeneity outcropping in the top layer. The real components of the base electric field, E_x, and magnetic field, H_x, were computed for these models at periods 1000 s and 100 s respectively. These results are compared with published results in figures 3(c–f).

The first inversion exercise was performed on the conductive block model of Agarwal *et al* (1993). This model consists of a conductive block embedded in the top resistive layer of a two layer model. The 20 km wide, 10 km thick block of resistivity 10 ohm m is at a depth of 10 km. The 40 km thick top layer of 100 ohm m resistivity is underlain by a conductive layer of 10 ohm m resistivity. The horizontal extent of the model grid was 200 km (−100 km to 100 km), while its vertical extent was 100 km (0 to 100 km). On the basis of the synthetic forward response, a 40 ohm m inversion domain, extending from −30 km to 30 km in horizontal direction and 5 km to 25 km in vertical direction, was identified. Since the body was best sensed at the 80 s period, the corresponding E-polarization impedance, Z_{xy}, was inverted. Both the real and imaginary components of the inverted model impedance closely fit the true values. The root mean square (rms) error during the inversion process continuously decreased with the increasing iteration number, signifying acceptability of the inversion

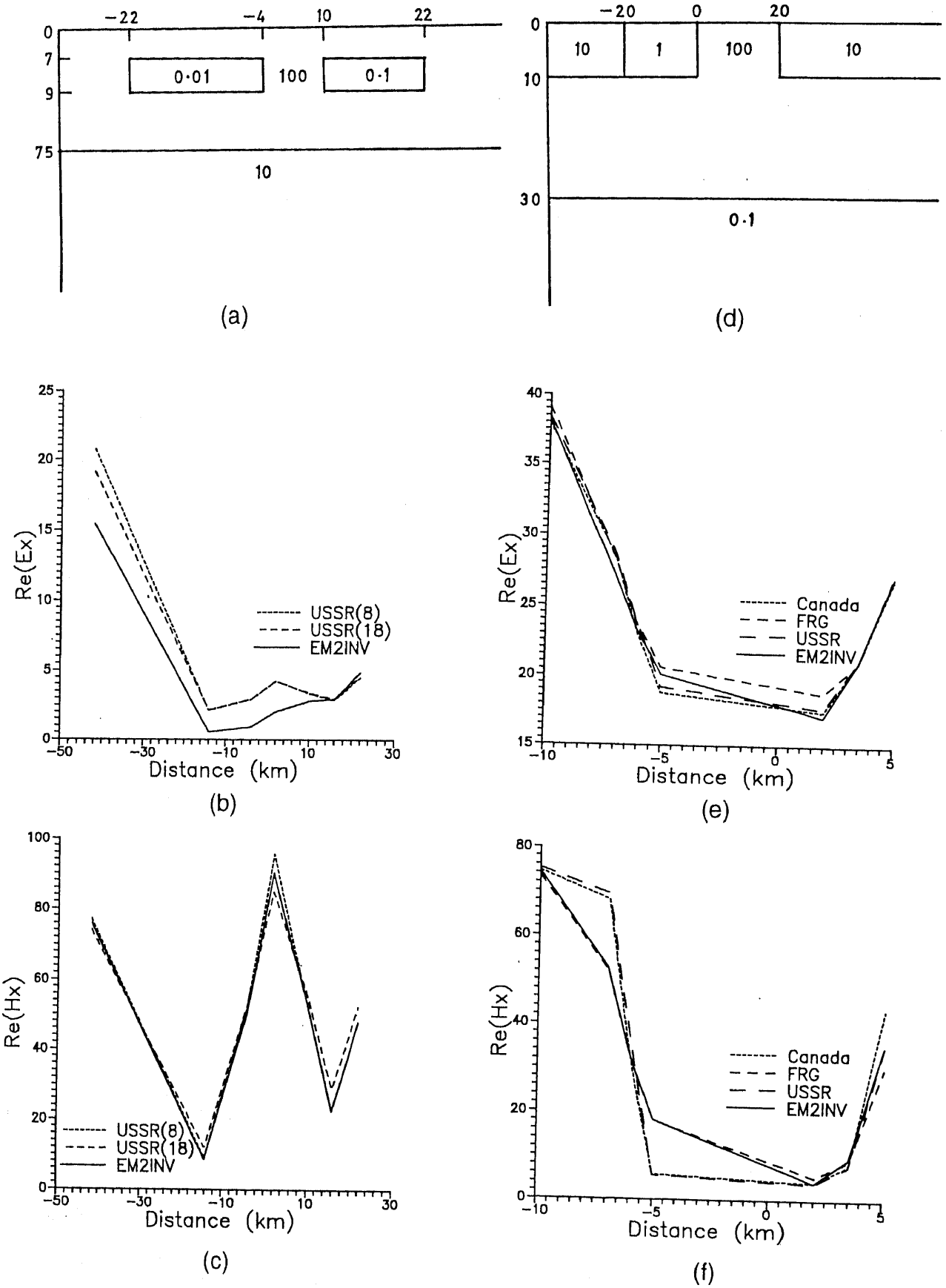

Figure 3. The two models chosen from report of Zhdanov *et al* (1990), (**a, d**). Comparison of EM2INV results with some of the results given in the report (**b, c**) and (**e, f**) are plots of real parts of E_x and H_x for the two models respectively.

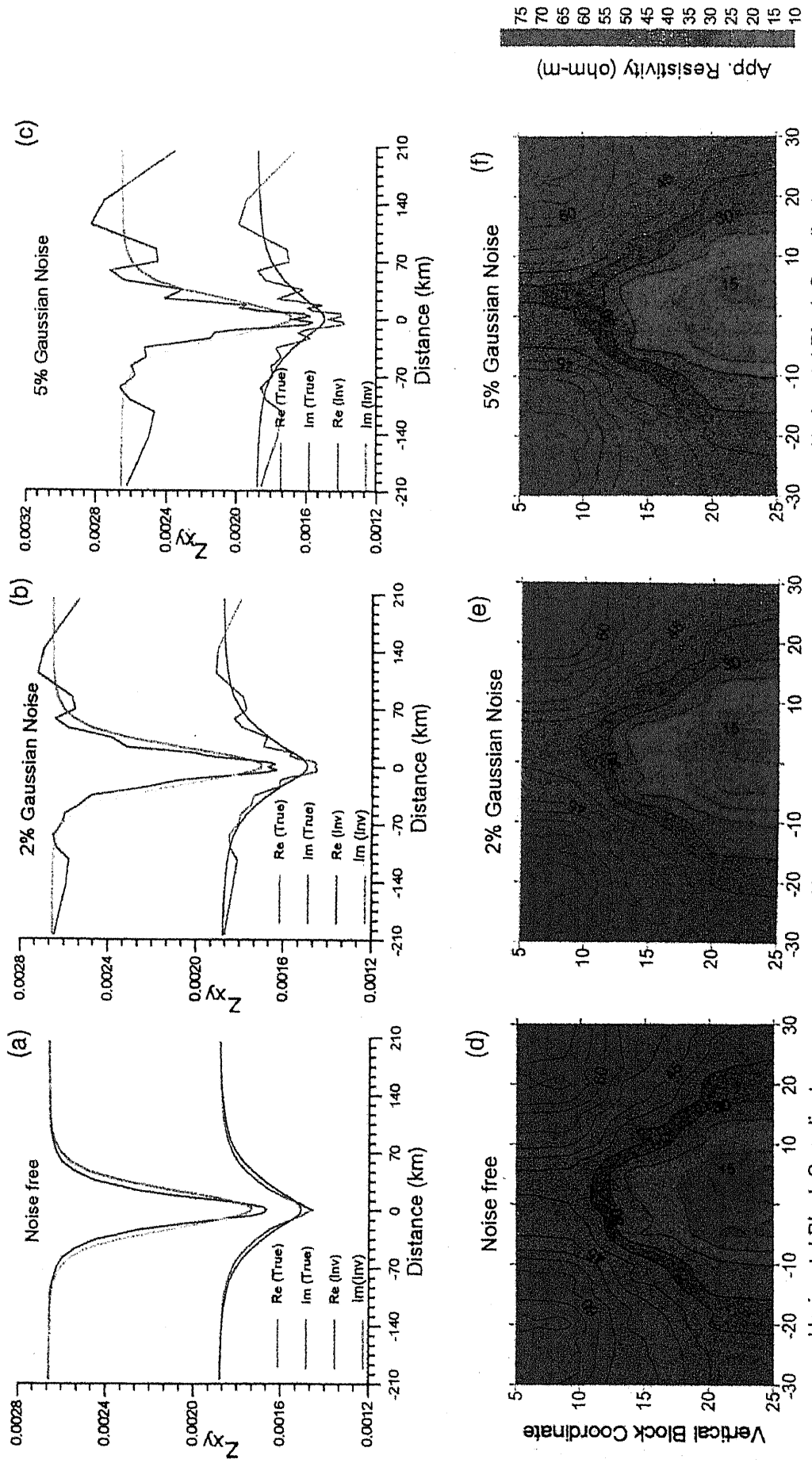

Figure 4(a–f). (*Continued*)

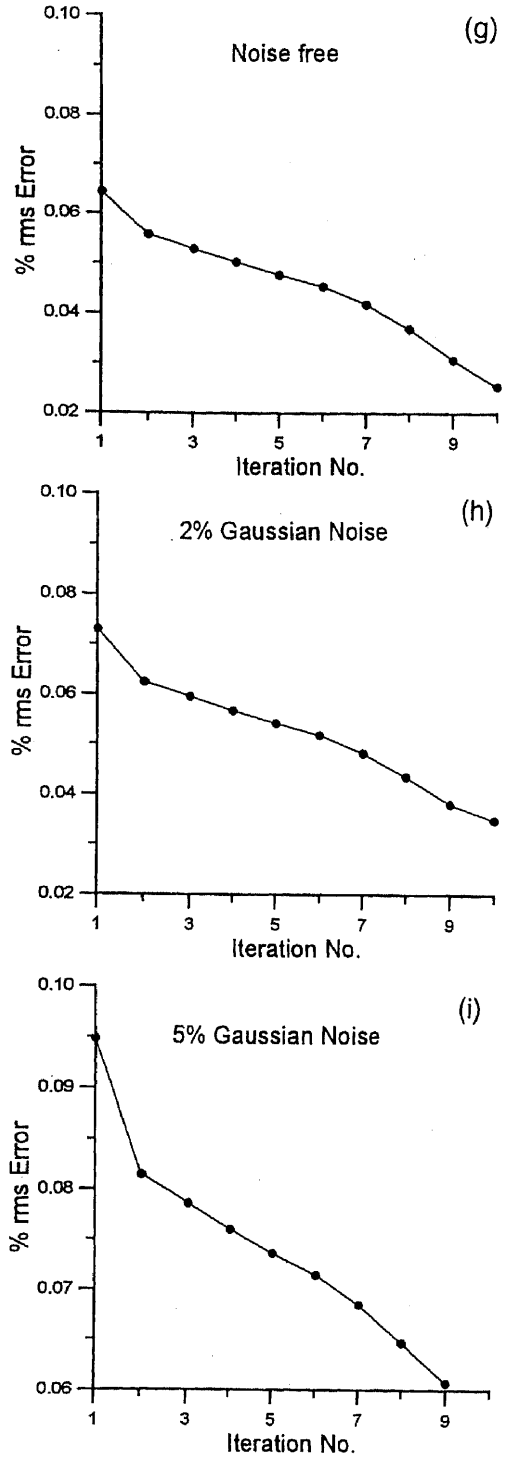

Figure 4. Inversion of synthetic Z_{xy} data for conductive block model with increasing random noise. The comparison of true and inverted model responses for (a) noise free, (b) 2% noise and (c) 5% noise. Parts (d)–(f) show the contours of resistivity (in ohm m) within inversion domain while parts (g)–(i) show the convergence of rms error in inversion for noise free, 2% and 5% noise respectively.

quality. The top horizontal and the two vertical boundaries of the body were well resolved. However, the bottom horizontal boundary could only be reasonably inferred. The inverse solution stability was studied by inverting the noisy data. Before inversion, random Gaussian noise of different signal to noise ratios were added to the synthetic response. The addition of noise resulted in high frequency oscillations in an otherwise smooth response curve. The inversion of different noisy Z_{xy} responses revealed that the quality of inverted model was acceptable as long as the noise level was $\leq 5\%$. The inversion results for 0%, 2% and 5% Gaussian noise cases are shown in figure 4. These results confirm the stability of EM2INV.

3.2 *Experiment design exercises*

The experiment design exercises performed, not only rigorously tested but also enhanced the algorithm's forward response generation as well as data inversion capabilities. For data inversion, the initial guess model is obtained from the observed anomaly. Hence, the forward modelling experiments were conducted with the goal of studying the impact of model parameters on the forward responses. The inversion experiments, on the other hand, were performed to gauge the inversion quality under different situations. Such experiments help in improving quality of inversion and also in planning data acquisition. Three two-layer earth models, with conductive and/or resistive block(s) buried in the top layer, were chosen from Agarwal *et al* (1993). Model 1, described in the previous section, has a conductive block, model 2 has a resistive block and model 3 has a pair of resistive-conductive blocks. Model 2 is similar to model 1, except for the block resistivity which is 1000 ohm m instead of 10 ohm m. In model 3, two blocks of width 10 km and thickness 10 km, having resistivities 10 ohm m and 1000 ohm m, are buried in a host of 100 ohm m. The separation between the two blocks is 40 km.

3.2.1 *Experiments with forward algorithm*

Parameters studied with models 1 and 2, were: (i) the contrast between the target and host resistivities (2, 5, 10, 100, 1000 for model 1 and 10, 50, 100 for model 2) and (ii) the depth to the top of the target (0, 10, 30, 40, 50 km). For model 3, the inter-block resistivity contrast and the horizontal separation (0, 10, 20, 40 km) were the key parameters studied. Since the body was sensed best at the period 80 s, all the responses were generated for this period. A careful study of these responses revealed that the anomaly peak sharpened with increasing resistivity contrast ratio. However, this sharpness was perceptible only up to a certain depth of burial beyond which even a large contrast ratio did not help in detection of the body. For a constant contrast ratio, the magnitude of anomaly was greater for the conductive block than for the resistive block. The conductive and resistive blocks

were better sensed by the E- and B-polarizations respectively. The model 3 responses clearly supported this observation because the corresponding ρ_{xy} curves did not reflect the presence of resistive block at all and instead, merged into the half-space values. The impact of the depth of burial was studied only on models 1 and 2. The apparent resistivities were computed at different depths of burial for a given resistivity contrast ratio. It was observed that due to attenuation of the signal, the magnitude of anomaly decreased with increasing depth of burial. This study revealed that for the burial depths greater than 30 km the almost flat 80 s period anomalies contained virtually no information about the target. The outcropping body was distinctly perceptible in the B-polarization responses due to a sudden jump in the ρ_{yx} values at the edges. This feature helped in estimating the horizontal extent of the body. The model 3 apparent resistivities ρ_{yx} and ρ_{xy} were computed, for a fixed contrast ratio, for different separation values. The effect of separation between the two blocks was reflected better in ρ_{yx} than in ρ_{xy}. For ρ_{xy}, this effect was perceptible only when the block was conductive in comparison to the host rock. As the block became resistive the response curves became almost identical for the different separation values.

3.2.2 *Experiments on inversion algorithm*

The inversion algorithm is a versatile one and can be used to invert various response functions. The profiling as well as the sounding data can be inverted equally efficiently. Numerous factors like choice of response function, mode of polarization, number of periods used for inversion, spread of observation points, individually or jointly affect the quality of inversion. In order to study these influences, some theoretical experiments were designed which, in turn, further established the efficacy of EM2INV. These exercises were conducted on models 1 and 2. Apart from using *a priori* information about the layered earth models (1D), better initial guess models were constructed on the basis of forward anomalies. For the models under consideration, the inversion domains encompassing the target extended from −30 km to 30 km horizontally and from 5 km to 25 km vertically. The assumed resistivities of the inversion domains for models 1 and 2 were 40 ohm m and 500 ohm m respectively. The grids used to invert the data were different from the ones used in the forward computations. During the inversion process, periods smaller than 10 s resulted in large numerical grids which could not be handled on the available computational facility. Therefore, we used 11 periods (in s)-10, 15, 20, 40, 80, 160, 320, 640 1280, 2560 and 5120 for generation of synthetic responses. The choice of standard frequency (period) was crucial because the inversion domain blocks of the corresponding grid were used as super-blocks in subsequent inversion iterations. For selection of the standard frequency, the single frequency inversion at each period of the given range was carried out. Since the inversion of the 80 s response was efficient, this particular period was taken as the standard one. The 31 grid points of the standard frequency grid, extending from −204 km to 204 km, were used as observation points for inversion. The observation points were (in km) −204, −144, −114, −99.3, −84.3, −69.3, −58, −46.7, −35.5, −24.2, −17.1, −13.6, −10, −6.6, −3.3, 0, 3.3, 6.6, 10, 17.1, 24.2, 35.5, 46.7, 58, 69.3, 84.3, 99.3, 114, 144, 204. The optimum value of the regression parameter was taken to be 0.1. The minimum-maximum limits of the resistivity values were 1–100 ohm m and 100–5,000 ohm m for models 1 and 2 respectively. Before undertaking the 2D inversion, the synthetic responses were corrupted with 2% random Gaussian noise.

The MT as well as GDS response functions, impedance and induction vector respectively, can be inverted using EM2INV. In order to analyze the relative performance of the impedance Z_{xy} and the induction vector I_{zy}, these responses were computed at the standard frequency for model 1 and then inverted. The responses computed for the inverted model fit the true Z_{xy} and I_{zy} responses. Although there was greater % rms error in the inversion of MT data, yet the target resistivity was better estimated than from the GDS data. The MT data resolved the exact depth of burial while the GDS data demarcated the horizontal extent of the target. Both the MT and the GDS data could not resolve the lower boundary of the body.

The next exercise aimed at studying the relative performance of the two modes of polarization of the MT data. For this purpose, the B- and E-polarization responses of models 1 and 2 were generated for the standard frequency and then inverted. For model 1, the inversion of Z_{xy} imaged the target better than that of Z_{yx}. On the contrary, the inversion results for model 2 indicated superior inversion of Z_{yx} response. The target got shifted upwards during the inversion of Z_{xy} response. For both the models, the lower end of the target was not clearly identified in either modes. The lateral boundaries were well imaged by inversion of Z_{yx} response for both the models. Thus, the conductive bodies were better resolved by inversion of E-polarization data while the resistive bodies by inversion of B-polarization data.

The different depth levels of inhomogeneity can be tapped by controlling the frequency which, in turn, controls the penetration depth. Generally, a large number of frequencies are used to improve the resolution. This results in overall increase of computation time that is linearly proportional to the number of frequencies used. A theoretical exercise that demonstrated the impact of the number of frequencies on the quality of inversion was devised. It also identified the

minimum number of frequencies necessary for performing an efficient inversion. These exercises were performed through the inversion of Z_{xy} response of model 1. Initially, the model response generated at the standard frequency was inverted using all the observation points. Subsequently, the number of frequencies was increased one by one. The period lying on either side of the standard frequency was selected from the given range 10 s–5120 s. The procedure was repeated till all the frequencies of the range were included and for each step the inversion was carried out. It was observed that with increasing number of frequencies, there was no remarkable difference in the inversion results. An increase in the number of frequencies continuously decreased the % rms error, but at a significant increase in computer time. These results established that if the extent of profile length was large enough to tap the target, then an increase in number of frequencies did not improve the inversion quality.

Besides the frequency, the spread of observation points also controls the penetration depth. Larger the spread deeper will be the penetration. An experiment, analogous to the previous one, which aimed at finding out the minimum number of observation points needed for a good quality inversion was carried out. Initially all the 31 observation points, extending from −204 km to 204 km, were used for inversion of Z_{xy}, at standard frequency. Gradually two observation points, one each from the flanks, were removed till only one observation point, the centre of the profile, was left. If the set of frequencies used was not able to invert the data properly then another frequency was added. The body was best resolved when inversion was performed using all the 31 observation points. However, even when very few (5 or 1) observation points, were used for inversion, it helped in deciphering the approximate model. The most interesting result was obtained when the inversion was carried out using only one observation point. These results illustrated that even a single observation point of the profile contained significant information about the body and yielded an approximate model after inversion. This result highlights the utility of the 2D inversion in comparison to the 1D inversion, where the single point data inversion provides only a layered earth model.

4. Examples

The algorithm EM2INV was first tested on several data sets derived from theoretical models simulating the basic structures, commonly encountered – horst, sill, dike, faulted block, conductive block, resistive block, salt dome, sedimentary basin etc. After a comprehensive literature survey, the 2D models, representing geologically meaningful situations, were selected. Various workers (Patra and Mallick 1980; Pek 1985; Madden and Mackie 1989; Oldenburg 1990; Zhdanov *et al* 1990; Smith and Booker 1991; Agarwal *et al* 1993) have given simple 2D geophysical models. The results presented here pertain to the two models – coductive and resistive pair model (model 3) embedded in two-layer earth (Agarwal *et al* 1993) and the sedimentary basin model (model 4, Madden and Mackie 1989). One field example from Central Himalaya has already been published (Rastogi *et al* 1998) and that may be seen in conjunction with the present paper for completeness.

A study, to ascertain whether the stacked 1D models can be improved further by 2D inversion or not, was conducted on the models taken from Agarwal *et al* (1993). As a result, the inversion became a two step procedure. In the first step, the 1D inversion was carried out at each observation point for given time periods and then the inverted 1D models were stacked to derive the initial 2D model. In the second step 2D inversion was performed to get the final model. The straightforward inversion scheme (SIS) (Gupta *et al* 1996) was used for the first step while EM2INV was used in the second step. SIS requires the number of layers in the model and the constant layer thickness in unit of layer skin depth. The number of layers assumed was in general 100. For EM2INV, the inversion domain encompassing the true body and its resistivity was defined on the basis of the 1D stacked model. The forward responses, computed for the given period range at specific observation points and corrupted with 2% Gaussian noise, were used as data for SIS. For EM2INV, only the significant periods, for which the body was better sensed, were used. For a general model with 9 observation points and 6 periods, the CPU time taken for SIS was about 120 seconds per observation points while for EM2INV, using all the observation points and 2 periods, the time taken was about 816 seconds.

The response for model 3, to be used in SIS and EM2INV, were calculated for the same 11 periods as for model 1. The number of sites were increased to 19 (in km) as −100, −75, −50, −40, −35, −30, −25, −20, −10, 0, 10, 20, 25, 30, 35, 40, 50, 75 and 100, to cover full width of the region containing the anomalous bodies. The domain used for 2D inversion extended from −40 km to 40 km horizontally and from 10 km to 25 km vertically. Since the inversion of the starting model with a depth of burial different from the true one did not succeed, the exact burial depth of blocks was taken. The assumed resistivities of inversion domain were 150 ohm m and 30 ohm m respectively for both Z_{yx} and Z_{xy} inversions. The basic inversion results, the pseudosections and the resistivity contours, resulting from the 1D and 2D inversions are shown in figure 5. The Z_{yx} inversion better indicated the presence of the resistive block (figure 5(b) and 5(d)) while the Z_{xy} inversion reproduced the con-

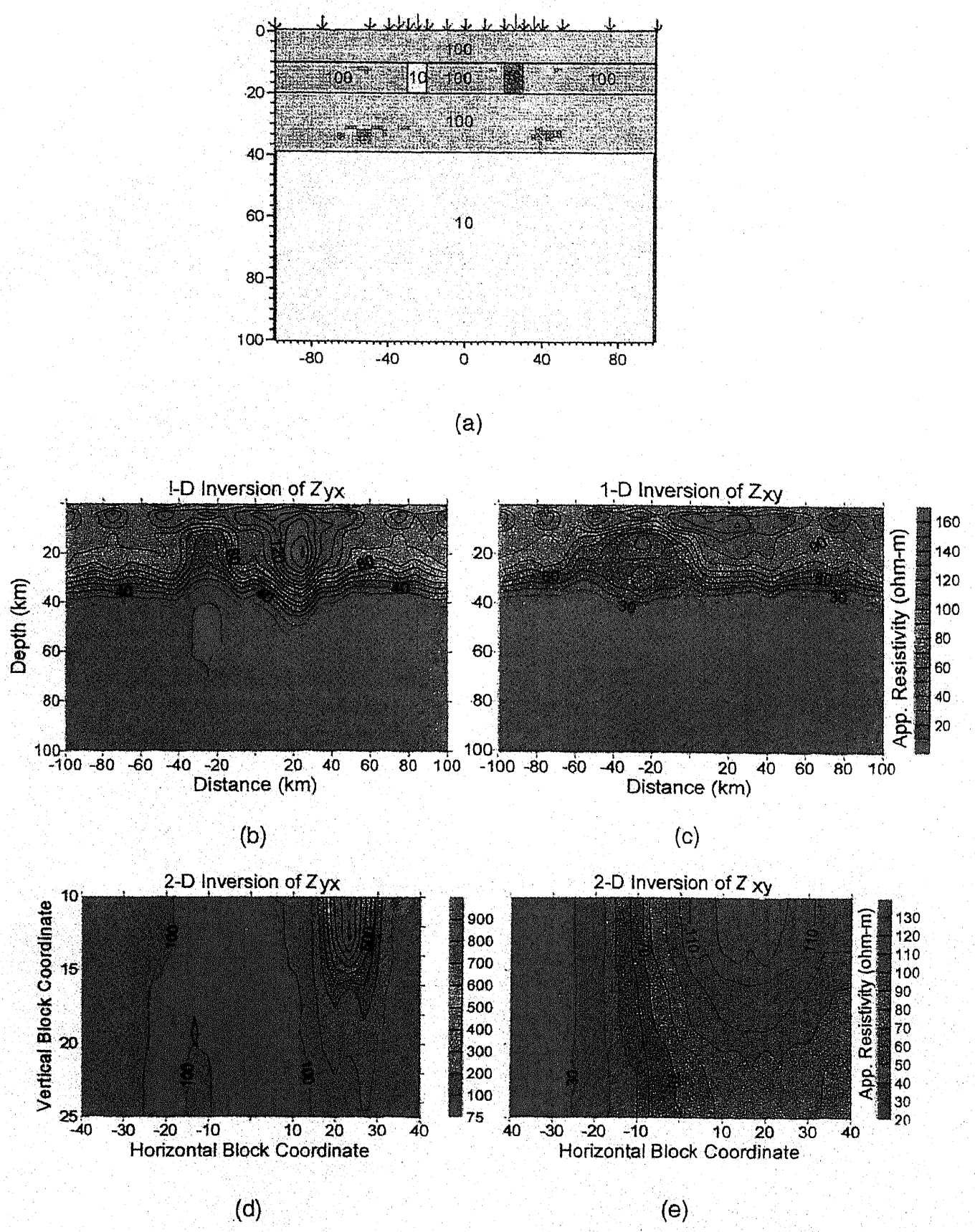

Figure 5. (a) Conductive and resistive block model with positions of observation points marked on the horizontal axis by arrows, (b) and (c) the pseudosections obtained from SIS for the B- and E-polarization, (d) and (e) resistivity contour plots of model obtained from EM2INV for B- and E-polarization.

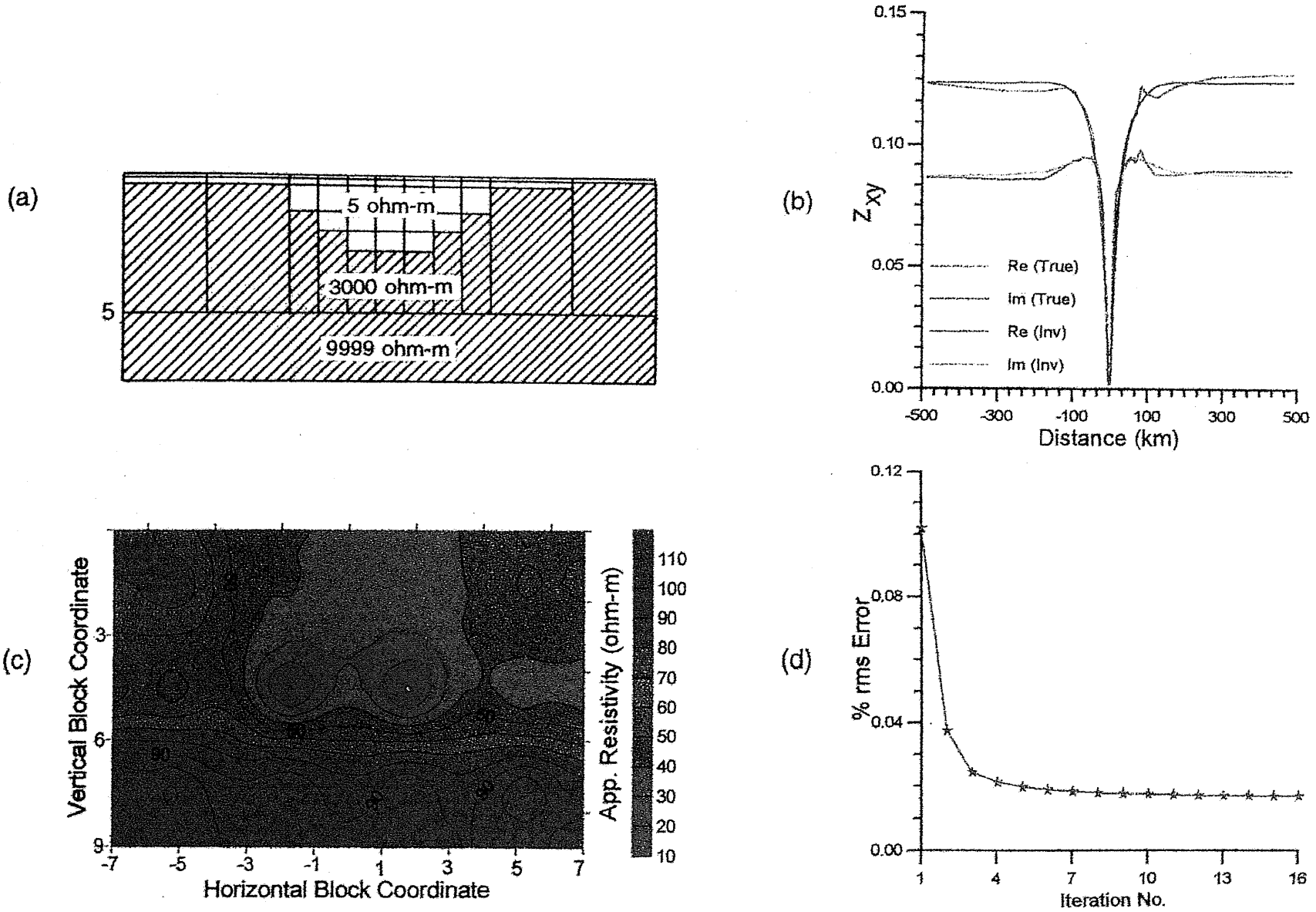

Figure 6. (a) Sedimentary basin model with 2:1 vertical exaggeration (after Madden and Mackie 1989). (b) Comparison of true and computed Z_{xy} response. (c) Resistivity contour plots of inverted model obtained from inversion of Z_{xy} response. (d) Convergence of the inversion iterations for inverted model.

ductive block more prominently (figure 5(c) and 5(e)). Figures 5(d) and 5(e) present the 2D resistivity contours and further support this observation by giving better estimates of resistivities. This exercise illustrates that the results of B- and E-polarization are complimentary to each other and can be used for estimating the true model in a comprehensive manner.

The inversion of the response of a simple basin model 4, used by Madden and Mackie (1989) was performed by directly using EM2INV. Figure 6(a) depicts the 2D model with a 2 : 1 vertical exaggeration. The conductive basin of 5 ohm m resistivity was buried in a resistive host of 300 ohm m. A numerical value 9999 ohm m was assigned to the highly resistive basement. Since the model was conductive, the inversion of Z_{xy} scored over that of Z_{yx}. Moreover, in this particular case, the inversion results of Z_{yx} were not very satisfactory. Hence, results of Z_{xy} only are presented here. The forward response was computed for period 10 s and inversion was carried out using all the grid points as observation points. Based on *a priori* information from the 1D model and the forward anomaly, the inversion domain was taken from −7 km to 7 km and 0 km to 9 km in horizontal and vertical directions respectively. The resistivity was assumed to be 100 ohm m. The misfit between the true and inverted responses, the resistivity contour and the % rms error are given in figures 6(b), 6(c) and 6(d) respectively. The response of the inverted model matched with the true Z_{xy} response. The inverted model was able to identify the bottom boundary of the basin. Being Z_{xy} inversion, the resistivity was underestimated in the vertical model (figure 6c). The % rms error was high in the first iteration. As soon as the true parameter values were approached in subsequent iterations, the error estimates reduced and convergence was achieved after few more iterations (figure 6d).

5. Conclusions

The algorithm EM2INV, presented in this paper, constitutes an efficient and reliable software package for the inversion of 2D geoelectromagnetic data. The algorithm has been rigorously and comprehensively tested. All the studies conducted to investigate the efficacy of this algorithm yielded encouraging results. The comparison of the results of EM2INV with those obtained using other existing algorithms, highlighted the efficiency of the algorithm. This justified a qualified faith in the algorithm. Primarily from the results of experiment design exercises and from the inversion studies carried out on different data sets, the following conclusions can be drawn:

- The choice of time periods, employed for data acquisition, should not only be constrained by the skin depth but also by the spread of observation points, i.e. length of the profile. If the profile length is sufficiently large then increase in number of periods does not improve the inversion quality.
- For a wide spectrum of frequencies, even a single observation point on the profile contains significant information about the inhomogeneity. 2D inversion of such data set does yield an approximate model.
- Inversion of MT data provides better estimates of the vertical variation whereas GDS data deciphers the horizontal variations better.
- The conductive and resistive bodies are better resolved by inversion of the E- and B-polarization responses respectively.
- The localization of vertical boundaries is better achieved by inversion of the B-polarization data in comparison to the E-polarization data which are good in demarcating the horizontal boundaries.
- The inverted resistivity values are overestimated in the B-polarization data, in comparison to those obtained by the E-polarization data.
- An initial guess model derived from 1D stacked results substantially improves the inversion quality in comparison to the one using the initial guess model on the basis of the 2D forward anomaly.

Acknowledgements

The authors duly acknowledge the financial support provided by the Council of Scientific and Industrial Research, New Delhi, in the form of a research project.

References

Agarwal A K, Poll H E and Weaver J T 1993 One- and two-dimensional inversion of magneto-telluric data in continental regions; *Phys. Earth Planet. Inte.* **81** 155–176

Axxelson O 1980 Conjugate gradient type methods for unsymmetric and inconsistent system of linear equations; *Linear Algebra Appl.* **29** 1–16

Brewitt-Taylor C R and Weaver J T 1976 On the finite difference solution of two-dimensional induction problems; *Geophys. J. Roy. Astr. Soc.* **47** 375–396

Chen P F and Fung P C W 1989 A mesh convergence test for the finite difference method in three-dimensional electromagnetic modelling; *Chinese J. Geophys.* **32** 569–573

deGroot-Hedlin C D and Constable S C 1990 Occam's inversion to generate smooth, two-dimensional models from magneto-telluric data; *Geophysics* **55** 1613–1624

EMSLAB 1988 The EMSLAB electromagnetic sounding experiment; *Eos. Trans. AGU* **69** 89–99

EMSLAB 1989 Special issue of JGR devoted to the EMSLAB experiment; *J. Geophys. Res.* **94** 14093–14283

Gupta P K, Benett L A and Raiche A P 1987 Hybrid calculations of the three-dimensional electromagnetic response of buried conductors; *Geophysics* **52** 301–306

Gupta P K, Sri Niwas and Gaur V K 1996 Straightforward inversion scheme (SIS) for one-dimensional magneto-telluric data; *Proc. Indian Acad. Sci. (Earth Planet Sci.)* **105**, 413–429

Hibbs R D and Jones F W 1976 The calculation of perturbation and induction arrows for a three-dimensional conductivity model and dipole source fields; *PAGEOPH* **114** 997–1008

Hohmann G W 1971 Electromagnetic scattering by conductors in the earth near a line source of current; *Geophysics* **36** 101–131

Jacobs D A H 1981 Preconditioned conjugate gradient algorithm for solving finite different system; In: *Sparse matrices and their uses-* (ed) Ian S Duff (Springer-Verlag) 509–535

Jacobs D A H 1986 A generalization of the conjugate gradient method to solve complex system; *IMA J. Numr. Anal.* **6** 447–452

Jones F W and Pascoe L J 1971 A general computer program to determine the perturbation of alternating electric currents in a two-dimensional model of a region of uniform conductivity with an embedded inhomogeneity; *Geophys. J. R. Astr. Soc.* **24** 3–30

Jones F W and Pascoe L J 1972 The perturbation of alternating geomagnetic fields by three-dimensional conductivity inhomogeneties; *Geophys. J. Roy. Astr. Soc.* **27** 479–485

Jupp D L B and Vozoff K 1977 Two-dimensional magneto-telluric inversion; *Geophys. J. R. Astr. Soc.* **50** 333–352

Kershaw D S 1978 The incomplete Cholesky-conjugate gradient method for the iterative solution of system of linear equations; *J. Comput. Phys.* **26** 43–65

Lee K H, Pridmore D F and Morrison H F 1981 A hybrid three-dimensional electromagnetic modelling scheme; *Geophysics* **46** 796–805

Mackie R L and Madden T R 1993 Conjugate direction relaxation solution for 3D magneto-telluric modelling; *Geophysics* **58** 1052–1057

Mackie R L, Madden T R and Wannamaker P E 1993 Three-dimensional magneto-telluric modelling using difference equations; *Geophysics* **58** 215–226

Mackie R L, Smith J T and Madden T R 1994 Three-dimensional electromagnetic modelling using finite difference equations: The magneto-telluric example; *Radio Science* **29** 923–935

Madden T R and Mackie R L 1989 Three-dimensional magneto-telluric modelling and inversion; *Proc. IEEE* **77** 318–333

Meijerink J A and van der Vorst H A 1977 An iterative solution method for linear systems of which the coefficient matrix is a symmetric M-matrix; *Math. Comp.* **31** 148–162

Nabighian M N (Ed) 1988 Electromagnetic methods in applied geophysics, vol. I, Theory; *SEG* 528 pp

Oldenburg D W 1979 One dimensional inversion of natural source magneto-telluric observations; *Geophysics* **44** 1218–1244

Oldenburg D W 1990 Inversion of electromagnetic data: An overview of new techniques; *Geophys. Surv.* **11** 231–270

Oldenburg D W and Ellis R G 1993 Efficient inversion of magneto-telluric data in two-dimensions; *Phys. Earth Planet. Inte.* **81** 177–200

Parker R L 1977 Understanding inverse theory; *Annu. Rev. Earth Planet. Sci.* **5** 35–64

Parker R L and Whaler K A 1981 Numerical methods for establishing solutions to the inverse problem of electromagnetic induction; *J. Geophys. Res.* **85** 9574–9584

Patra H P and Mallick K 1980 Geosounding principles, 2: Time-varying geoelectric soundings; (Amsterdam: Elsevier) 419 pp

Patrick F W and Bostick F X Jr 1969 Magneto-telluric modelling technique; *Rep. 59 Elec. Geophys. Res. Lab.* University of Texas Austin

Pek J 1985 Linearization methods of interpreting magneto-telluric and magnetic variation data; *Travaux Inst. Geophys. Acad. Tchecosi. Sci.* **609** 199–326

Raiche A P 1974 An integral equation approach to three-dimensional modelling; *Geophys. J R. Astr. Soc.* **36** 363–376

Rastogi A 1997 A finite difference algorithm for two-dimensional inversion of geoelectromagnetic data; *Ph D Thesis* University of Roorkee, Roorkee

Rastogi A, Gupta P K and Sri Niwas 1998 Inversion of GDS data of northwest Himalaya using EM2INV; *Proc. Indian Acad. Sci. (Earth Planet. Sci.)* **107** 149–154

Reddy I K, Rankin D and Phillips R J 1977 Three-dimensional modelling in magneto-telluric and magnetic variational sounding; *Geophys. J Roy. Astr. Soc.* **51** 313–325

Reid J K 1971 On the method of conjugate gradients for the solution of large systems of equations; In: *Proc. Conf. Large sparse sets of linear equations*; (ed) J K Reid (Academic Press) 231–254

Rodi W L, Swanger H J and Minster J B 1984 ESP/MT: An interactive system for two-dimensional magneto-telluric interpretation (Abstract); *Geophysics* **46** 611

Sarkar T K (ed) 1991 Application of conjugate gradient method to electromagnetic and signal analysis; (Amsterdam: Elsevier Science Publ. Co.)

Sarkar T K, Yang X and Arvas E 1988 A limited survey of various conjugate gradient methods for solving complex matrix equations arising in electromagnetic wave interactions; *Wave Motion* **10** 527–546

Sasaki Y 1989 Two-dimensional joint inversion of magneto-telluric and dipole-dipole resistivity data; *Geophysics* **50** 254–262

Smith J T 1996a Conservative modelling of 3D electromagnetic fields, Part I: Properties and error analysis; *Geophysics* **61** 1308–1318

Smith J T 1996b Conservative modelling of 3D electromagnetic fields, Part II: Biconjugate gradient solution and an accelerator; *Geophysics* **61** 1319–1324

Smith J T and Booker J R 1991 Rapid inversion of two- and three-dimensional magneto-telluric data; *J. Geophys. Res.* **96** 3905–3922

Ting S C and Hohmann G W 1981 Integral equation modelling of three-dimensional magneto-telluric response; *Geophysics* **46** 182–197

Wannamaker P E 1991 Advances in three-dimensional magneto-telluric modelling using integral equations; *Geophysics* **56** 1716–1728

Wannamaker P E, Hohmann G W and San Filipo W A 1984 Electromagnetic modelling of three-dimensional bodies in layered earth using integral equations; *Geophysics* **49** 60–74

Weaver J T 1994 Mathematical methods for geoelectromagnetic induction; Research Studies Press Taunton

Weaver J T and Agarwal A K 1993 Automatic one-dimensional inversion of magneto-telluric data by the method of modelling; *Geophys. J Int.* **112** 115–123

Weaver J T and Brewitt-Taylor C R 1978 Improved boundary conditions for the numerical solution of E- polarization problems in geomagnetic induction; *Geophys. J Roy. Astr. Soc.* **54** 309–317

Weaver J T, Pu X H and Agarwal A K 1996 Improved methods for solving for the magnetic field in E-polarization induction problems with fixed and staggered grids; *Geophys. J. Int.* **126** 437–446

Weidelt P 1972 The inverse problem of geomagnetic induction; *Zeit. fur Geophysik* **38** 257–289

Weidelt P 1975 Inversion of two-dimensional conductivity structures; *Phys. Earth Planet. Inte.* **10** 282–291

Whittal K P and Oldenburg D W 1992 Inversion of magneto-telluric data for one-dimensional conductivity; *Geophysical Monograph Series* No. 5 (ed) D V Fitterman SEG Tulsa Oklahoma

Xinghua P, Agarwal and Weaver J T 1991 A theoretical investigation of anisotropic geoelectric structures using three-dimensional models; *XX General Assembly* IUGG Vienna

Xiong Z 1992 Symmetry properties of the scattering matrix in 3D electromagnetic modelling using integral equation method; *Geophysics* **57** 1199–1201

Yamane K, Takasugi S and Lee K H 1996 A new magneto-telluric inversion scheme using generalized RRI; *J. App. Geophys.* **35** 209–213

Zhdanov M S and Fang S 1996 Quasi-linear approximation in 3D electromagnetic modelling; *Geophysics* **61** 646–665

Zhdanov M S, Varenstov E M, Golubev N G and Kriulov B A 1990 Modelling methods for electromagnetic fields; *International Material Project COMMENI* Nauka Moscow

MS received 27 September 1999; revised 19 November 1999